LASER CLADDING OF NANOCRYSTALLINE ALLOY BASED ON CAST IRON WITH NIOBIUM AND BORON ADDITIONS

Felipe Amélio de Lucena[1,2]
Claudemiro Bolfarini [3]
Cláudio Shyinti Kiminami [3]
Conrado Ramos Moreira Afonso [3]
[1]Programa de Pós-Graduação em Ciência e Engenharia de Materiais (PPG-CEM), Universidade Federal de São Carlos (UFSCar), Rodovia Washington Luís, km 235 – SP 310, CEP 13565-905, CP 676, São Carlos – SP, Brazil
[2]Instituto Federal de São Paulo (IFSP), Catanduva – SP, Brazil
felipe.lucena@ifsp.edu.br
[3]Departamento de Engenharia de Materiais (DEMa), Universidade Federal de São Carlos (UFSCar), Rodovia Washington Luís, km 235 – SP 310, CEP 13565-905, CP 676, São Carlos – SP, Brazil
cbolfa@ufscar.br, kiminami@ufscar.br, conrado@ufscar.br

Abstract. *Amorphous and nanocrystalline Fe-based alloys present excellent properties, such as high hardness and wear resistance, with cooling rates of* 10^3 *to* 10^5 *K/s. Thus, this study aims obtain nanocrystalline or metastable structure through rapid solidification (RS) of white cast iron with B and Nb additions, resulting in composition* $(Fe_{65}Cr_{17}Mo_2C_{14}Si_2)_{88}Nb_4B_8$ *(%at), and the overspray powder was used to produce coatings of ferrous metallic alloys on AISI 1020 mild steel substrate by laser cladding of the pre-placed powders. The ferrous alloy was processed through Melt-Spinning, the Discovery® Plasma copper mold casting (CMC) and Spray Forming (SF) obtaining ribbons (40 µm thick), plates (1.0 and 2.0 mm) (CMC) and powders (20 to 180 µm) of* $(Fe_{65}Cr_{17}Mo_2C_{14}Si_2)_{88}Nb_4B_8$ *(%at) alloy. Different laser parameters, power (200, 400 and 600 W), scanning speeds (6.7-150.0 mm/s), were tested using a Yb fiber laser (2 kW) and the products were characterized by scanning electron microscopy (SEM), X-ray diffraction (XRD), differential scanning calorimetry (DSC) and measurements of Vickers microhardness. The characterization showed amorphous ribbons, nanocrystalline atomized powders, plates (mm) and clad tracks with nanocrystalline phases: α-Fe, γ-Fe,* Cr_7C_3*, FeNbB e* Fe_2B*. Laser clad coatings showed Vickers microhardness ranging 820 – 1270 HV depending on laser parameters and respective power density (W/mm*^{2}*).*

Keywords: *Laser Cadding, Cast Iron, Spray forming, Rapid Solidification, Characterization*

1. INTRODUCTION

Nanocrystalline and metastable alloys have been investigated due to their improved mechanical, physical and chemical properties over crystalline materials. Besides the development of nanocrystalline alloys, new processing routes have been also investigated. The spray forming process is one of such new routes (Afonso, 2004). Spray forming, also named spray casting or spray deposition, is the inert gas atomization of a liquid metal stream into variously sized droplets which are then propelled away from the region of atomization by the fast flowing, atomizing gas. Fe-based amorphous and nanocrystalline alloys have been studied for industrial applications because of their rich resources and low costs. Atomized powders of Fe-based alloys can then be used to produce nanocrystalline coatings on steel substrate, improving corrosion properties in aggressive environments (Koga, 2014), such as chemical industries and oil refineries.

Laser Cladding is an advanced surface modification technique for production of metallurgically well-bonded coatings used for adding one material to the surface of another in a controlled manner enabling the applied material to be deposited selectively just where it is required (Vilar, 1999; Vilar, 2001; Zhang, 2011). Laser cladding makes the non-equilibrium synthesis of the clad layer to the substrate possible due to its rapid cooling rates of about 10^4 K/s (Aghasibeig, 2012). The surface treatments through laser for advanced applications can improve wear and corrosion resistance of the materials through significant improvements in its properties (Gargarella, 2014). The laser processing of advanced metallic materials presents advantages, such as, reduction in operational costs, quality improvement and finishing of products, etc (Maier, 1992). The Ferrous alloy composition of this study was based in a white cast iron $Fe_{65}Cr_{17}Mo_2C_{14}Si_2$ (%at) with 4at%Nb and 8at%B additions to the global nominal composition of the alloy, resulting in the $(Fe_{65}Cr_{17}Mo_2C_{14}Si_2)_{88}Nb_4B_8$ (%at) alloy.

In the present study we studied different laser parameters to produce coatings from overspray powders produced by spray forming (SF) process based on amorphizable $(Fe_{65}Cr_{17}Mo_2C_{14}Si_2)_{88}Nb_4B_8$ (%at) alloy over low carbon steel (AISI 1020) substrate by laser cladding. The microstructure, phase composition and Vickers microhardness of the transversal section of the single clad tracks and the surface of superimposed of the clad tracks were investigated.

2. EXPERIMENTAL PROCEDURE

The $(Fe_{65}Cr_{17}Mo_2C_{14}Si_2)_{88}Nb_4B_8$ (%at) alloy was chosen as coating material due to possibility of obtaining a nanocrystalline structure combining duplex matrix of ferrite (Fe-α) and Fe-γ (austenite) with hard carbides Cr_7C_3 and borides Fe_2B and FeNbB intermetallic phases. The overspray powders were prepared by spray forming (Afonso, 2007), with grain size ranging from 20-180 µm. Laser cladding was carried out by the pre-placed powder method on square substrates of AISI 1020 mild steel with a size of 100 × 100 × 6 mm. The coatings precursors were prepared by placing a 0.2 mm thick layer onto substrate. These layers were melted and clad with the laser beam under different parameters, power (W), scanning speed (mm/s) and focal length (mm) resulting in a variation of the power density (PD – J/mm^2). The aim was to select the parameters that allowed amorphous phase formation with minimal dilution while still creating a metallurgical bonding with the substrate and to characterize the microstructure, phase composition, glass formation and microhardness of clad tracks. Laser cladding experiments were conducted with Yb Fiber Laser (up to 2 kW) IGP in a high-purity argon gas atmosphere. The microstructure of the clad tracks was analyzed by optical microscopy, using an Olympus PMG3 microscope, and scanning electron microscopy (SEM), with a FEI Inspect S50 and Philips XL30 FEG. The phases formed in the clad tracks were analyzed by X-ray diffraction (XRD) using a Siemens D5005 diffractometer and Cu-K_α radiation. The analysis was conducted in a flat area created at the surface of the superimposed clad tracks (around 10 × 10 mm) and at the transversal section of clad tracks by metallography technique. The glass transition, crystallization and melt temperatures (T_g, T_x and T_m) were determined using a differential scanning calorimeter (DSC) Netzsh 404, at a heating rate of 40.0 K/min. The microhardness of the clad tracks was measured with a HMV-2000 Shimadzu microhardness tester and a Vickers pyramid-shaped diamond indenter, under different loads from 0.05 (50.0 g) up to 2.0 kg.

3. RESULTS AND DISCUSSION

Figure 1 presents X-ray diffraction (XRD) pattern of coating obtained from atomized powder in different size ranges (<20, 20–45, 45–106, 106–180 and >180 µm) and for the millimeters thick deposit of $(Fe_{65}Cr_{17}Mo_2C_{14}Si_2)_{88}Nb_4B_8$ (%at) alloy at Power = 200 W and V = 25 mm/s.

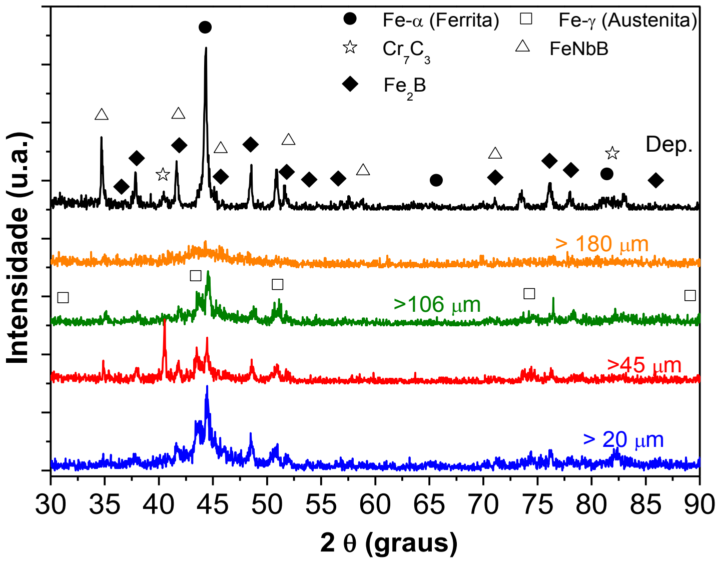

Figure 1. X-ray diffraction (XRD) pattern of coating obtained from atomized powder in different size ranges (<20, 20 – 45, 45 – 106, 106 – 180 and > 180 µm) and for the milimiters thick deposit of $(Fe_{65}Cr_{17}Mo_2C_{14}Si_2)_{88}Nb_4B_8$ (%at) (%at) alloy at Power = 200 W and 25 mm/s.

Figure 2. SEM images in backscattered electrons mode (BSE) of surface morphology of the atomized powders in different size ranges of (a) 20-45 µm and (b) 45-106 µm for $(Fe_{65}Cr_{17}Mo_2C_{14}Si_2)_{88}Nb_4B_8$ (%at) alloy. To estimate the influence of laser parameters on the penetration depth of the coating material on the AISI 1020 mild steel substrate and in the microhardness of the coatings, several single clad tracks were produced on the substrate and characterized by different techniques, as can be seen further. Different laser parameters, power (W), scanning speed (mm/s) and focal length (mm) were investigated, which produced single clad tracks from the application of different power densities (PD – J/mm^2), laser useful optical power, on to pre-placed powders.

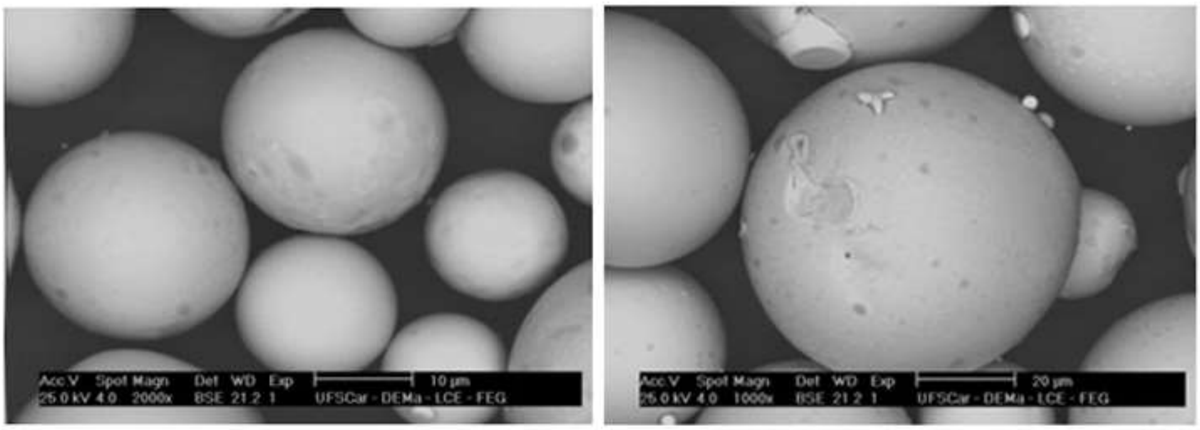

Figure 2. SEM images in backscattered electrons mode (BSE) of surface morphology of the atomized powders in different size ranges of (a) 20-45 µm and (b) 45-106 µm for $(Fe_{65}Cr_{17}Mo_2C_{14}Si_2)_{88}Nb_4B_8$ (%at) alloy.

Table 1. Laser parameters, power and scanning speed, used in the laser surface treatment. Calculated values to the power density (PD) and values measured to penetration depth and microhardness.

$(Fe_{65}Cr_{17}Mo_2C_{14}Si_2)_{88}Nb_4B_8$ (%at) Atomized Powder				
Power (W)	Scanning speed (mm/s)	Penetration depth (µm)	PD (J/mm^2)	Hardness (HV)
200	25,0	—	8,0	1175 ± 53
200	16,7	—	12,0	1169 ± 66
200	13,3	—	15,0	1183 ± 37
200	10,0	—	20,0	1172 ± 63
200	6,7	1	29,9	1266 ± 89
400	25,0	—	16,0	846 ± 47
400	16,7	—	24,1	895 ± 63
400	13,3	—	30,1	1044 ± 54
400	10,0	—	40,0	1150 ± 40
400	6,7	—	59,7	1203 ± 83
600	25,0	—	24,0	822 ± 63
600	16,7	—	36,1	889 ± 45
600	13,3	0.5	45,1	955 ± 67
600	10,0	4.7	60,0	1020 ± 25
600	6,7	5.3	89,6	1191 ± 44
200	150,0	—	1,3	1104 ± 66
200	100,0	—	2,0	1220 ± 76
200	66,7	—	3,0	1292 ± 31

In this work, for PD calculations, it was used values of laser beam diameters of 0.5 or 1.0 mm, calculated by Eq. (1), for the $(Fe_{65}Cr_{17}Mo_2C_{14}Si_2)_{88}Nb_4B_8$ (%at) alloy, respectively, which depend on the focal length used. Herein were used focal lengths of 4.0 and 8.0 mm, respectively, for $(Fe_{65}Cr_{17}Mo_2C_{14}Si_2)_{88}Nb_4B_8$ (%at) nanocrystalline alloy.

$$W(Z) = W_0 \left[1 + \left(\frac{\lambda Z M^2}{\pi (W_0)^2}\right)^2\right]^{\frac{1}{2}} \quad (1)$$

Where: W is radius beam, W_0 is minimum radius in focal plane (100 µm), λ is wavelength (1070 nm), Z is relative distance to the focal plane and M^2 is quality factor (22.4). Then, the PD values were calculated, according to Eq. (2), for each group of laser parameters and showed in Table 1

$$PD\left(\frac{J}{mm^2}\right) = \frac{Power\ (W)}{Scanning\ speed\ \left(\frac{mm}{s}\right) \times Beam\ diameter\ (mm)} \quad (2)$$

Vickers microhardness measurements of the transversal section of single clad tracks of the $(Fe_{65}Cr_{17}Mo_2C_{14}Si_2)_{88}Nb_4B_8$ (%at) coatings produced by laser cladding on the AISI 1020 mild steel substrate are depicted in Figs. 1(a)-(b). The Vickers microhardness measurements were performed using 50 g load ($HV_{0.05}$) and the single clad tracks were produced using the laser parameters showed in the Tab. 1.

The Vickers microhardness analysis of $(Fe_{65}Cr_{17}Mo_2C_{14}Si_2)_{88}B_8Nb_4$ (%at) coatings, Fig. 1(a), showed that the single clad tracks produced with the same scanning speed, 25.0 – 6.7 mm/s, didn't present increase in the average microhardness. When the laser power increased, the average microhardness decreased. Figure 1(a), for example, shows that for scanning speed 25 mm/s, the average microhardness of single clad tracks was 1175 ± 53, 846 ± 47 and 822 ± 63 HV, for laser power 200, 400 and 600 W, respectively. These results indicated that the single clad tracks obtained with lower laser power (200 W) showed greater hardness values, irrespective of scanning speed. Analyzing the average microhardness of single clad tracks produced with the same laser power, 200 W (harder than 400 and 600 W), and different scanning speeds, 25.0 – 6.7 mm/s, it can be seen in the Fig. 1(a) that the average microhardness increase as the scanning speed increase, for example, the average microhardness of single clad tracks was 838 ± 79, 1060 ± 53 and 1184 ± 104 HV, at 30, 50 and 100 mm/s, respectively.

$(Fe_{65}Cr_{17}Mo_2C_{14}Si_2)_{88}Nb_4B_8$ (%at)

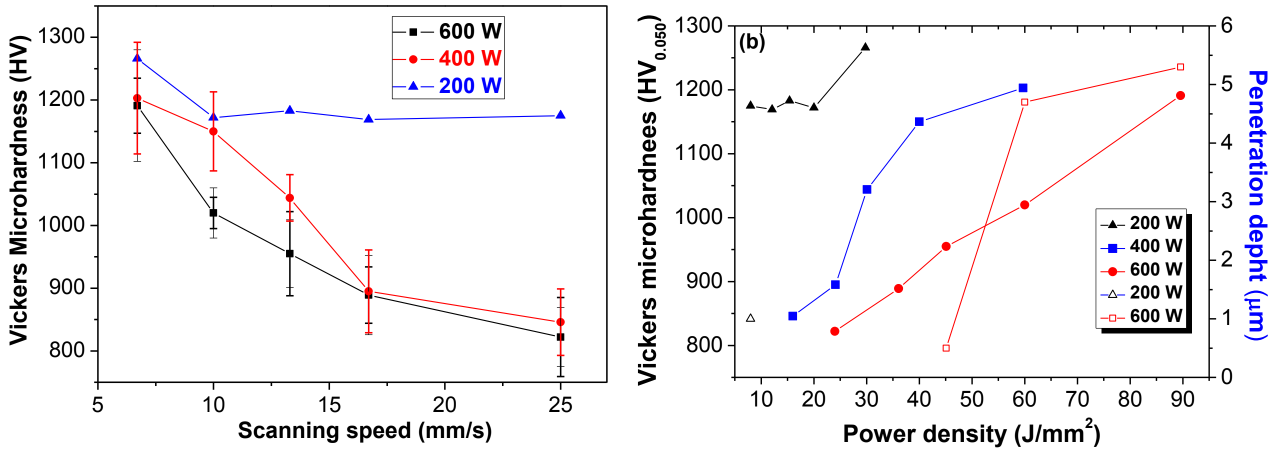

Figure 3. Vickers microhardness measurement of the transversal section of clad tracks obtained from (a) $(Fe_{65}Cr_{17}Mo_2C_{14}Si_2)_{88}Nb_4B_8$ (%at) alloy, both with different laser powers and scanning speeds. Figure 2. Variation of Vickers microhardness in function of power density (PD) and penetration depth of the transversal section of clad tracks obtained from $(Fe_{65}Cr_{17}Mo_2C_{14}Si_2)_{88}Nb_4B_8$ (%at) alloy.

For cooper mold cast samples of $(Fe_{65}Cr_{17}Mo_2C_{14}Si_2)_{88}Nb_4B_8$ (%at) alloy obtained in plate shape for thickness of 1 and 2 mm, the microhardness values obtained were 1339 ± 61 and 1483 ± 31 HV, respectively. For spray formed deposits the measurement of microhardness showed not so high values of around 1050 HV in average for milimiters thick deposit. That lower value is due probably to high fraction of porosity (~5%), typical of spray forming process. Laser cladding tracks obtained for $(Fe_{65}Cr_{17}Mo_2C_{14}Si_2)_{88}Nb_4B_8$ (%at) alloy and scanning speeds of 6.7 up to 150 mm/s lead to an increase of the microhardness values of coatings (ranging from 800 up to ~1300HV), reaching almost maximum values of cooper mold cast samples. It must be stressed that the recovered of AISI 1020 mild steel substrate with the $(Fe_{65}Cr_{17}Mo_2C_{14}Si_2)_{88}B_8Nb_4$ (%at) alloy confer to substrate higher resistance to permanent deformation. Moreover, the Vickers microhardness values were much larger than substrate, 160 ± 10 HV (Gargarella, 2014).

Figures 2(a)-(b) show the variation Vickers microhardness values and penetration depth of the coating material on the substrate with PD, of transversal section of the single clad tracks obtained from $(Fe_{65}Cr_{17}Mo_2C_{14}Si_2)_{88}Nb_4B_8$ (%at) alloys, both with different laser parameters (Tab. 1). The penetration depth was measured using confocal optical microscopy. However, when Nb was added to alloy composition, $(Fe_{65}Cr_{17}Mo_2C_{14}Si_2)_{88}Nb_4B_8$ (%at) alloy, SEM analysis showed that the penetration depth of the coating material on the steel substrate was imperceptible or very small, irrespective of laser parameters, probably due to higher viscosity of nanocrystalline alloy. For example, Tab. 1 and Fig. 2(b), show that with laser power 600 W the PD values ranged from 9.0 to 36.1 J/mm^2 and the penetration depth of the coating material on the steel substrate ranged from 0.5 to 5.3 µm. It must be stressed that although the penetration depth of the coating material on the steel substrate is small, always should exist a metallurgical bonding with the substrate.

For the $(Fe_{65}Cr_{17}Mo_2C_{14}Si_2)_{88}Nb_4B_8$ (%at) alloy, Fig. 2(a), was observed that the Vickers microhardness values measured increased as PD and penetration depth decreased, for the same laser power. In addition, the Vickers microhardness values decreased as the laser power applied increased due to high penetration depth, which makes more material of the metal base blends with the coating, changing its properties. Therefore, was observed that the higher Vickers microhardness values were obtained from the lower laser power, 200 W. According to the results obtained by SEM and XRD analyses, in this condition was observed higher volume fraction of the amorphous phase in the other cases. It must be stressed that the greater the amorphous fraction formed, in general, higher the hardness of the crystalline coatings (Gargarella, 2014).

Figure 2(b) shows, in general, that Vickers microhardness values measured were constant, according to standard deviation, irrespective laser parameters, except for lower PD's, 4.0, 6.0 and 9.0 J/mm^2, with laser power 600 W and PD 6.0 J/mm^2 with laser power 200 W. Therefore, was observed that the higher Vickers microhardness values were obtained from laser power 200 W, irrespective laser parameters, and laser power 600 W with small PD's, according to standard deviation. The results obtained above showed that Co addition and the increase in the B content (Gargarella, 2014) in the alloy composition, increased the Vickers microhardness values of the coatings produced with the same laser parameters. However, for laser power 200 W, where higher volume fraction of the amorphous phases was observed, the Vickers microhardness values of the coatings, in general, were the same, according to standard deviation.

3.1 X-ray diffraction (XRD) analysis of the coatings

The X-ray diffractograms of the superimposed surface of clad tracks for $(Fe_{65}Cr_{17}Mo_2C_{14}Si_2)_{88}Nb_4B_8$ (%at) alloys are presented in Figs. 3(a) and 3(b), respectively. The XRD patterns of superimposed surface clad tracks for $(Fe_{65}Cr_{17}Mo_2C_{14}Si_2)_{88}Nb_4B_8$ (%at) alloy, Fig. 3(a), were produced at different laser parameters that resulted in PD = 8 J/mm^2 with overlaps 0.4 mm and laser spot diameter = 1.0 mm.

The XRD pattern presented low intensity peaks that could be identified in the were: ferrite Fe-α, austenite Fe-γ, Fe_2B, Cr_7C_3 and FeNbB intermetallic phases (Kim, 2015). The increase in the intensity of Fe-α peak as the laser power increase was due to nanocrystal growth. The results obtained herein, indicated that the most favorable condition to obtain nanocrystalline coating of $(Fe_{65}Cr_{17}Mo_2C_{14}Si_2)_{88}B_8Nb_4$ alloy at scanning speed of 25 mm/s combined with lower laser power (200 W). The diffractogram showed a typical pattern for nanocrystalline structure with low intensity set of peaks, but the one produced at lower scanning speed, 10 mm/s, presented a broad peak which was indexed as Fe-α phase together with the appearance of the amorphous halo around this peak.

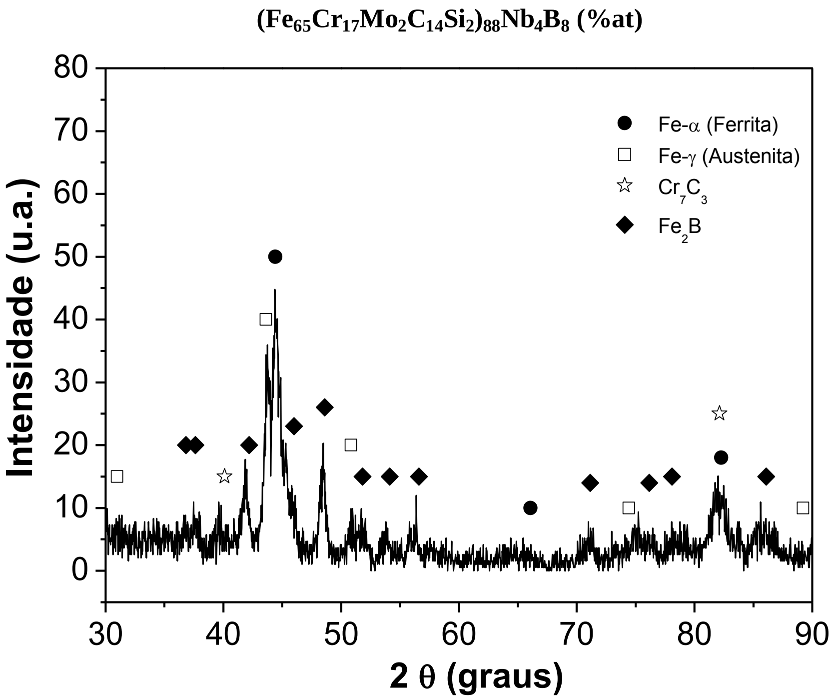

Figure 4. X-ray diffraction pattern of coating obtained from superimposed clad tracks of atomized powder of $(Fe_{65}Cr_{17}Mo_2C_{14}Si_2)_{88}Nb_4B_8$ (%at) alloy at Power = 200 W and 25 mm/s.

Figure 3(b) shows that among the diffractograms produced with PD's 12.0, and 24.0 J/mm^2, i.e., same scanning speed, 16.7 mm/s, and different laser powers, 200 W (TS3 with overlap 0.5 µm) and 400 W (TS4 with overlaps 0.5 and TS5 with 1.0 µm), respectively, only one produced at lower laser power (200 W) presented a broad peak that was indexed as Fe-α phase together with the baseline elevation and appearance of an amorphous halo around this peak. As mentioned previously, the amorphous halo is characteristic of a nanocrystalline structure of the Fe-α phase embedded in the remaining amorphous phase. In other cases, the XRD patterns showed crystalline coatings, but, it must be stressed that the enlargement of the peaks indicates that they present low crystallinity. The peaks observed were indexed as equilibrium phases, Fe-α, Fe_2B - Reference code: 36-1332 (JCPDS, 2000), and FeNbB (Kim, 2015). It can be seen that increasing B content from 15.0 at% to 19.0 at% was sufficient to change the phase composition of single clad track, through appearance of another boride phase, Fe_2B.

This results indicated that the most favorable condition to obtain amorphous coatings of $(Fe_{65}Cr_{17}Mo_{2}C_{14}Si_{2})_{88}Nb_{4}B_{8}$ (%at) nanocrystalline alloy at scanning speed 16.7 mm/s was with lower laser power (200 W). Since the most suitable laser power to produced amorphous coating of $(Fe_{65}Cr_{17}Mo_{2}C_{14}Si_{2})_{88}Nb_{4}B_{8}$ (%at) alloy was laser power 200 W, it was tested lower scanning speeds, 6.7 mm/s, PD 29.8 J/mm^2 (TS1) and 10 mm/s, PD 20.0 J/mm^2 (TS2), and these scanning speeds as well is favorable to production of high hardness nanocrystaline coatings than with 16.7 mm/s. In both cases, the diffractograms showed crystalline coatings, which present sharp peaks, which were indexed as equilibrium phases, Fe-α, Fe_2B and FeNbB. As previously mentioned, these phases were not observed when the scanning speed was 16.7 mm/s, except Fe-α phase.

3.2 Microstructural analysis of the coatings

Figure 5 shows SEM images in backscattered electrons mode (BSE) of single clad tracks transversal section of $(Fe_{65}Cr_{17}Mo_{2}C_{14}Si_{2})_{88}Nb_{4}B_{8}$ (%at) alloy with the pre-placed powder showing the microstructure of the clad track – general view and coating/substrate interface: (a) and (b) Power = 200 W and scanning speed= 25 mm/s; (c) and (d) 400 W and 25 mm/s. (e) and (f) 600 W and 25 mm/s; (c) and (d) 200 W and 6,7 mm/s.

The microstructures of the single clad tracks produced with lower laser power, 200 W, at different scanning speeds of 100, 50 and 30 mm/s, showed that only the one produced with 100 mm/s was satisfactory, since at lower scanning speed, the coatings presented continuity failures or high porosity due to gas entrapment during the cladding process, which images were not shown here. The single clad track produced at laser power 200 W with 100 mm/s, (lower penetration depth of coating material on the steel substrate), showed that no crystalline phases (Fig. 5.a) were observed, indicating maintenance of glassy phase due to high GFA of this alloy. Furthermore, this result was in agreement with the XRD analysis (TS2100, Fig. 5.a) where the XRD patterm show low intensity peaks typical of nanocrystalline structure, indicating great refinement of microstructure. However, although there is amorphization evidence, in the coating/substrate interface it is possible to see, in the Fig. 5.b, dendrites of Fe-α phase dispersed in eutectic matrix and FeNbB intermetallic phase, indicating epitaxial growth from the steel substrate. In addition, the heat-affected zone (HAZ) formed in the substrate was narrow, but it is still possible to observe a change in the gray scale of the phases as it moves up from the steel substrate to the coating. The Fig. 5.c showed crystalline microstructure of the steel substrate near the interface.

Coatings produced at laser power 600 W with different scanning speeds, Figs 5.a to 5.c, showed that in these cases, the microstructure presented porous, small crystalline phases (FeNbB intermetallic phases) and coating/substrate interface with dendritic phases (150 and 100 mm/s) and granular dendrite morphology (30 mm/s). In addition, for both cases, Figs. 5, occurred nanocrystallization of the single clad tracks, as can be seen, FeNbB intermetallic phase appeared. The coatings presented cellular morphology and showed higher fraction of dendrites dispersed in the eutectic matrix indicating refinement with increase of penetration depth (dilution) of the coating material on the steel substrate (Fig. 2.a).

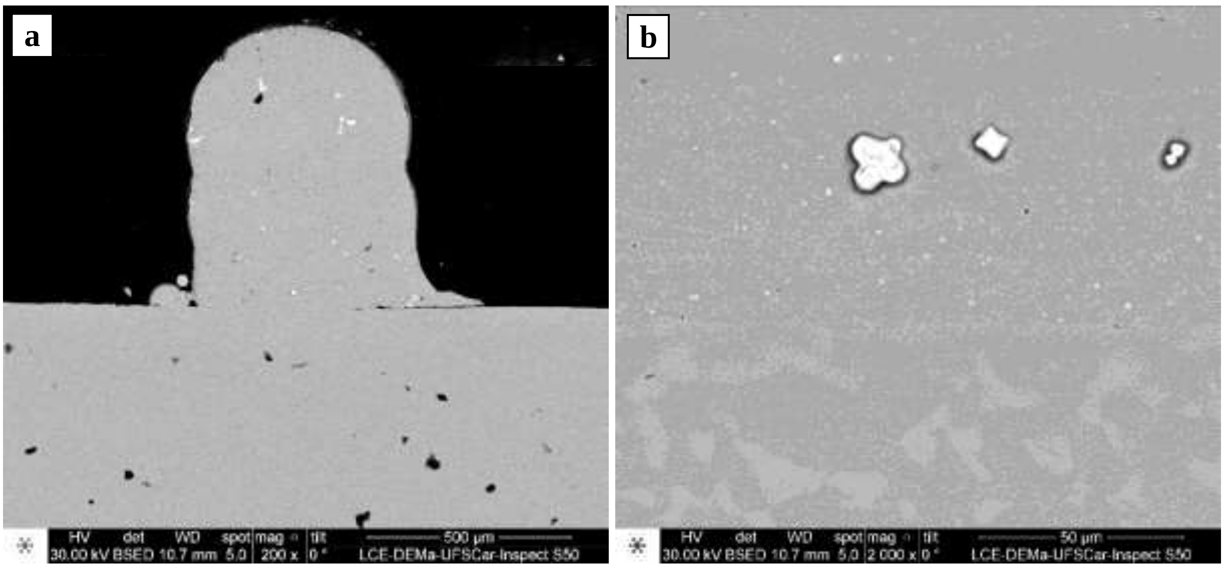

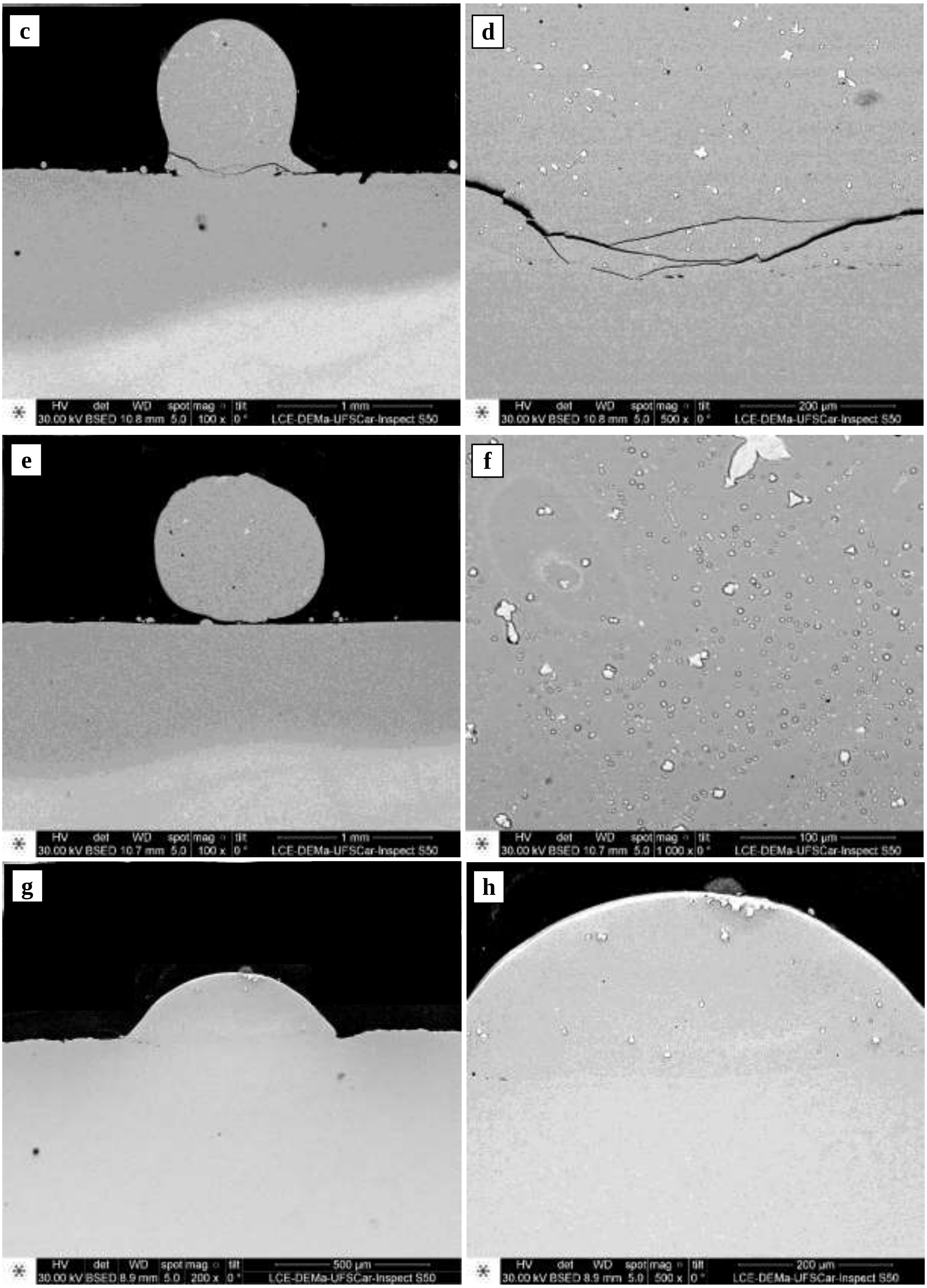

Figure 5. SEM images in backscattered electrons mode (BSE) of single clad tracks transversal section of $(Fe_{65}Cr_{17}Mo_{2}C_{14}Si_{2})_{88}Nb_{4}B_{8}$ (%at) alloy with the pre-placed powder showing the microstructure of the clad track – general view and coating/substrate interface: (a) and (b) Power = 200 W and scanning speed= 25 mm/s; (c) and (d) 400 W and 25 mm/s. (e) and (f) 600 W and 25 mm/s; (c) and (d) 200 W and 6,7 mm/s.

SEM analysis of the transversal section of single clad tracks of the $(Fe_{65}Cr_{17}Mo_2C_{14}Si_2)_{88}Nb_4B_8$ (%at) alloy obtained from different laser parameters showed in Tab. 1 are presents in the Figs. 5.a to 5.f. The microstructures of the clad tracks were very similar, irrespective of laser parameters, and the photomicrographs showed that occurred more crystallization of the coatings compared to the $Fe_{72}Nb_4Si_9B_{15}$ (at%) alloy. In all cases, it was observed nanocrystalline phases. Figure 5 shows that the coating presented small light phases, which can be attributed to nanocrystalline FeNbB intermetallic and small dark phases attributed to nanocrystalline Fe_2B intermetallic. The Figs. 5.b and 5.d show high magnification the nanocrystalline FeNbB intermetallic phases dispersed in the eutectic matrix indicating refinement of clad tracks. In the Fig. 5.e it can be seen a microstructure and composition transition between the clad track and steel substrate through the HAZ. In addition, the coatings exhibited an excellent interfacial bonding with the steel substrate. Finally, Fig. 5.f shows the dendritic epitaxial growth in the coating/substrate interface.

4. CONCLUSIONS

Rapid solidification of $(Fe_{65}Cr_{17}Mo_2C_{14}Si_2)_{88}Nb_4B_8$ (%at) alloy processed by melt-spinning (10^6 K/s), resulted in 100% amorphous structure in the micrometer thick ribbons and partially amorphous structure in the overspray powders produced by the spray forming process (10^3 – 10^5 K/s), diameters < 106 µm and >180 µm. The process of copper mold casting (10^3 K/s), and deposit (10^2 K/s) formed during spray forming fine crystalline microstructure.

Regarding laser cladding of $(Fe_{65}Cr_{17}Mo_2C_{14}Si_2)_{88}Nb_4B_8$ (%at) alloy For cooper mold cast samples of $(Fe_{65}Cr_{17}Mo_2C_{14}Si_2)_{88}Nb_4B_8$ (%at) alloy obtained in plate shape for thickness of 1 and 2 mm, the microhardness values obtained were 1339 ± 61 and 1483 ± 31 HV, respectively. For spray formed deposits the measurement of microhardness showed not so high values of around 1050 HV in average for milimiters thick deposit. That lower value is due probably to high fraction of porosity (~5%), typical of spray forming process. Laser cladding tracks obtained for $(Fe_{65}Cr_{17}Mo_2C_{14}Si_2)_{88}Nb_4B_8$ (%at) alloy and scanning speeds of 6.7 up to 150 mm/s lead to an increase of the microhardness values of coatings (ranging from 800 up to ~1300HV), more than 300%) higher than white cast iron, due to combination of refined and hard intermetallic carbide and borides: Cr_7C_3, FeNbB e Fe_2B and Fe-α (ferrite) matrix.

5. ACKNOWLEDGEMENTS

The authors gratefully acknowledge the financial support of the Brazilian institutions FAPESP (São Paulo State Research Foundation) Pos-doctoral Grant (2014/13432-9) and Research Project 2012/18429-0.

6. REFERENCES

Afonso CRM, Bolfarini C, Botta WJ, et al. Spray forming of the glass former $Fe_{83}Zr_{3.5}Nb_{3.5}B_9Cu_1$ alloy. *Materials Science and Engineering*. 2004;375-377:571-576.

Afonso CRM, Kaufma MJ, Bolfarini C, Botta Filho W, Kiminami CS. Gas Atomization of Nanocrystalline $Fe_{63}Nb_{10}Al_4Si_3B_{20}$ Alloy, *Journal of Metastable and Nanocrystalline Material*. 2004; 20-21:175-182.

Suryanarayana C, Inoue A. Bulk Metallic Glasses. Boca Raton: LLC, 2011. Capítulo 2.

Bonavina LF, Bolfarini C, Botta WJ, et al. Microstructural characterization of spray formed $Fe_{66}B_{30}Nb_4$ alloy. *Journal of Alloys and Compounds*. 2010;495:417–419.

Catto FL, Yonamine T, Kiminami CS, et al. Amorphous phase formation by spray forming of alloys $[(Fe_{0.6}Co_{0.4})_{0.75}B_{0.2}Si_{0.05}]_{96}Nb_4$ and $Fe_{66}B_{30}Nb_4$ modified with Ti. *Journal of Alloys and Compounds*. 2011;509S: S148–S154.

Gargarella, P., Almeida, A., Vilar R., Afonso, C.R.M., Peripolli, S., Rios, C.T., Bolfarini, C., Botta, W.J., Kiminami, C.S., 2014. "Formation of Fe-based glassy matrix composite coatings by laser processing". *Surface & Coatings*, Vol. 240, p. 336.

Grant PS. Spray Forming. *Progress in Materials Science*. 1995; 39:497-545.

Kui HW, Greer AL, Turnbull D. Formation of bulk metallic glass by fluxing. *Appl. Phys. Lett.* 1984;45:615–616.

Melle AK, Afonso CRM, Bolfarini C, et al. Microestrutura e resistência ao desgaste de aço recoberto com liga amorfizável $Fe_{60}Cr_8Nb_8B_{24}$ (%at), produzido por HVOF. *67° Congresso da ABM*. 2012.

Silva AMB. Produção de Recobrimentos Metálicos a partir de Ligas de Ferro Amorfizáveis. 2011. 105 f. *Dissertação* (Mestrado em Engenharia de Materiais) – Centro de Ciências Exatas e de Tecnologia, Universidade Federal de São Carlos, São Carlos, 2011.

7. RESPONSIBILITY NOTICE

The authors are the only responsible for the printed material included in this paper.